Int. J. Appl. Math. Comput. Sci., 2026, Vol. 36, No. 1, 37–51
DOI: 10.61822/amcs-2026-0004

BLDC MOTOR OUTPUT FEEDBACK VELOCITY TRACKING CONTROL WITH TRAPEZOIDAL APPROXIMATION AND NO ANGULAR VELOCITY STATE OBSERVER

CUAUHTÉMOC GUERRERO [a,*], VÍCTOR SANTIBAÑEZ [b], JORGE VILLALOBOS-CHIN [c], JORGE ORRANTE-SAKANASSI [b], JAVIER OLLERVIDES [b]

[a]Science and Technology College
Autonomous University of Mexico City
Prolongación San Isidro 151, Alc. Iztapalapa, C.P. 09790, Ciudad de México, Mexico
e-mail: cuauhtemoc.guerrero@uacm.edu.mx

[b]Division of Graduate Studies and Research
National Technological Institute of Mexico/La Laguna Institute of Technology
Blvd. Revolución y Av. Instituto Tecnológico de La Laguna, C.P. 27000, Torreón Coahuila, Mexico
e-mail: {vasantibanezd, jaorrantes, ejollervidesv}@lalaguna.tecnm.mx

[c]Faculty of Engineering, Sciences and Architecture
Durango State Juarez University
Calle Universidad, Gómez Palacio, C.P. 35070, Durango, Mexico
e-mail: jorge.villaloboschin@ujed.mx

In this work, a velocity tracking control strategy is presented using passivity methodology for a permanent magnet synchronous machine with uniformly distributed windings, which is known as a brushless direct current (BLDC) motor. The trapezoidal components of back electromotive force (EMF) are here modeled by using a novel differentiable approximation. The proposed control scheme is constructed by employing only measurements of the shaft position and stator currents. The use of a second-order filter makes it possible to solve the velocity tracking control problem without measuring the actual rotor velocity. A formal stability analysis of the closed-loop system consisting of the motor, the controller, and the second-order filter is presented using partial stability theory. By applying partial stability, the relevant variables are shown to converge, while the behavior of the rest of the variables that are not relevant to the control objective can be disregarded, which makes the theoretical analysis simpler. A numerical simulation is constructed to verify the applicability of the control law. The results show that all the variables of the BLDC motor are below the nominal values of the machine. Therefore, the physical implementation of the controller is feasible.

Keywords: BLDC motor, partial stability, second-order filter, trapezoidal approximation.

1. Introduction

Brushless DC (BLDC) motors are characterized by being highly efficient with high-power density, good velocity-torque characteristics, high-velocity operation capability, among other properties. Because of these characteristics, BLDC motors are widely used as a cost-effective solution in many small and medium motor drive applications, such as automotive and aerospace industries, as well as home and office equipment (Kim, 2017; Xia, 2012).

As to their physical structure, BLDC motors are three-phase AC synchronous ones, with uniformly spaced windings on the inside surface of the stator with two windings per phase (Chiasson, 2005), and because the usual way of driving such motors is by means of three-phase DC to AC converters (inverters) their windings are connected in star (Hanselman, 2006, Chapter 8). The magnetic fields are uniformly distributed in the

*Corresponding author

air gap of the motor (Chiasson, 2005; Nam, 2018). Due to this fact, at a constant angular velocity, BLDC back electromotive force (EMF) has a trapezoidal shape, unlike other motors such as permanent magnet synchronous ones (PMSMs), which have back EMF with a sinusoidal shape. For this reason, the BLDC motor is also known as trapezoidal back-EMF PM synchronous one.

In comparison to the PMSM, the BLDC motor has a lower cost and can be used in low-power, mass-produced applications (less than 5 KW) such as blowers, material handling equipment or domestic applications (Nam, 2018).

Likewise, the BLDC motor has proven to be a useful alternative over other electrical motors, especially induction ones (IMs). The two main reasons for this are as follows:

(a) The permanent magnets, made from rare earth elements, used in the construction of BLDC motors bring forth several benefits. For example, the steady-state performance of the motor is enhanced and its power density is increased. Additionally, the prices of rare earth magnets have been decreasing over time.

(b) The improvements made in the field of power semiconductors have facilitated the implementation of control schemes for the BLDC motor. The effective cost of the implementation of BLDCs motor is now lower in comparison with that of IMs (Gieras, 2009).

Another important benefit of BLDC motors is that they require less maintenance than other kinds of motors. This is due to their design, which does not include sliding rings or brushes. Therefore, the power losses in the rotor due to eddy currents are small. Power losses generally occur in stator windings. Consequently, adding cooling using a corrugated type structure in the motor casing can reduce such losses (Gieras, 2009).

Because of its structure, the BLDC motor is polyphase. The mathematical equations that describe the dynamics of the motor are highly nonlinear. Due to the latter, the control strategies initially applied to the BLDC motor were basically making some assumptions on the model to simplify it, i.e., proposed to use linear control techniques. In recent years, control algorithms have been introduced considering nonlinear control techniques, or in some cases a combination of both nonlinear and linear control strategies. Some of the main branches of study in the field of the control of BLDC motors can be classified as follows:

- *Controllers using PID actions.* The first algorithms used to solve the control problem for BLDC were PID control laws, considering a control loop for the electrical subsystem and another loop for the mechanical one. A trend in recent years is to use some of these control laws in combination with optimization techniques. For example, Jigang et al. (2019) employ a PI controller and the controller gains are tuned with an evolutional algorithm. In another work, to achieve velocity and torque control, the authors propose a fractional order PID controller optimized using the firefly algorithm (Kommula and Kota, 2020).

- *Direct torque control (DTC).* This technique provides a fast response to changes in the load torque as well as in the velocity reference. It is commonly used during transitions of different reference velocities, with the disadvantage of exhibiting an increased torque ripple (Carey *et al.*, 2019). There are several publications using this technique in combination with others. For example, Carey *et al.* (2019), employ DTC used in conjunction with field oriented control (FOC), obtaining advantages from both strategies. Another work (Khazaee *et al.*, 2020) applies the DTC technique to propose a control strategy obtaining a high-performance maximum torque per ampere (MTPA) considering the effect of iron losses. There are also proposals using DTC methodology as a foundation to perform power control, as is the case of Hajiaghasi *et al.* (2017), who applied a topology of only four power switches.

- *Fault tolerant control.* The inverter that supplies the power to the BLDC motor is subject to open circuit faults. Therefore, in order to overcome the aforementioned problem, fault-tolerant control strategies can be designed with an embedded fault diagnosis block. This is considered in some works, as is the case of Sova *et al.* (2015), who proposed a method that allows the operation of the BLDC motor under the failure of a hall sensor, whereas Salehifar and Moreno-Equilaz (2016) implemented a fault-tolerant control algorithm using finite set-model predictive control.

Other works consider the structure of the mathematical model of the BLDC motor and, when appropriate, present closed-loop stability proofs. Of these works, the following can be highlighted. First, de la Guerra *et al.* (2018), using the mathematical model with a trapezoidal back-FEM structure, propose an active disturbance rejection controller to compensate for the load torque variations in the shaft of the motor; working together, the BLDC motor controller and driver produce an unwanted torque ripple in the output torque. Taking into account this situation, in the work of Maharajan and Xavier (2018), a technique based on bioinspired algorithms is used to compensate or reduce

the torque ripple considering the trapezoidal model, whilst Hernández-Guzmán and Orrante-Sakanassi (2021) present a control scheme for direct drive BLDC motors coupled to a rigid robot with n-degrees of freedom. Such a work presents a global stability proof. In the paper by Guerrero *et al.* (2017), a velocity control scheme based on passivity was designed using the mathematical model of a BLDC motor with trapezoidal shapes of back EMF, taking the angular position as a measurement; by means of a second-order filter, an associated signal to the angular velocity was obtained. The global asymptotic stability of the closed loop system was thus accomplished.

The contributions of the present manuscript can be listed as follows. A velocity-tracking control scheme for the BLDC motor is presented. The passivity properties present in the mathematical model of the BLDC motor with trapezoidal shapes of back EMF are used to design the novel proposed control law with features that distinguish it from other controllers that have been developed for the BLDC motor, such as the following:

(a) Only the currents of the stator windings and the angular position of the rotor are considered as signals available for measurement, and they are used in the controller equations; this fact has been employed by both Guerrero *et al.* (2017) and Guerrero and Santibañez (2021). The former used such signals to implement velocity control for a BLDC motor, while the latter designed a velocity control law for a nonlinear DC motor. It is worth mentioning that, for these works, angular velocity is available instead of the angular position. Unlike the two aforementioned works, in this proposal, the equations for the velocity control voltages and the required stator currents are presented, which are obtained by using only signals from the available variables of the position and stator currents, which, due to their structure, are of great help in stability analysis.

(b) A signal associated to angular velocity is obtained by using a second order filter with relative degree equal to 1, where a state-space representation is applied. The second-order filter is similar to the one presented by Guerrero *et al.* (2017), with a different function used to represent the combination of the filter states. In practice, it is common to employ an optical encoder to obtain a signal regarding the position of the rotor of the electric motor. The signals that are obtained from the encoder may be processed to obtain an accurate measurement of the angular position. Therefore, angular velocity may not be as straightforward to measure. This can make the regulation and tracking of desired velocities a challenging task in BLDC motors.

(c) A function is constructed using the state-spaces variables from the second order filter implemented in the control law, i.e., it is employed to obtain both the control voltage equations and the equations required for the stator currents, unlike that employed by Guerrero and Santibañez (2021), which only is needed in the armature current equation that in turn is required by the control voltage of the armature windings of the nonlinear DC motor. Such a function is used in the stability analysis of the whole system.

(d) A quasi-trapezoidal vectorial function is designed which contains continuous and differentiable functions dependent on the angular position, i.e., these are similar to the trapezoidal functions present in the mechanical and electrical model of the BLDC motor, with the advantage being that quasi-trapezoidal functions are smooth and continuously differentiable in the transition of slope. Such a feature is necessary in the stability proof. Quasi-trapezoidal functions are constructed using trigonometrical ones, while those presented by Hernández-Guzmán and Orrante-Sakanassi (2021) are smoothed in the vertices with semicircles. It is worth mentioning that these quasi-trapezoidal functions were explicitly built to be used in the BLDC motor velocity proposed controller, to avoid discontinuity issues, and therefore, they are continuously differentiable.

(e) The desired currents in stator windings are obtained from the quasi-trapezoidal vectorial function, the desired angular velocity, the time derivative of the desired angular velocity, and the function obtained from the state-space variables of the second order filter.

(f) The analytical term of the time derivative of the desired currents requires angular velocity; however, a similar term is constructed using the desired angular velocity and the state associated to the second order filter and employed in the equation of the control voltages of the BLDC motor, similar to that presented by Guerrero and Santibañez (2021), who used it for the equation of the armature voltage of the nonlinear DC motor.

(g) The control signals are the motor supply voltages, and require the desired stator currents, the new similar term of the time derivative of the desired currents, the quasi-trapezoidal function, the desired angular velocity, and the current errors. That is, this proposal is very different from those that have traditionally been reported and widely used, since many proposals usually consider current profiles (commands) by means of current PI loops that only take into account a structure of the mechanical

dynamics of the machine to obtain rotor velocity control, e.g., as proposed by Chiasson (2005), instead of considering both mechanical and electrical dynamics, as in our poposal.

(h) A formal stability analysis of the complete closed-loop system is presented using partial stability theory, i.e., the relevant variables are shown to converge while the behavior of the other variables that are not relevant to the control objective, such as the rotor position and the filter states, can be disregarded, which makes the theoretical analysis simpler; to this end, Lemma 1 is originally introduced and formally proven.

(i) The proposed control law can be implemented with the technological devices available today.

2. Preliminaries

In this section, a lemma that will be used to prove the stability of the proposed control scheme is presented. It establishes sufficient conditions for the partial stability of a class of systems.

Consider a system of differential equations given by

$$\dot{\boldsymbol{x}} = \boldsymbol{f}(\boldsymbol{x}, t), \tag{1}$$

where $\boldsymbol{x} \in \mathbb{R}^n$, $t \in \mathbb{R}_+$, and $\boldsymbol{f} : \mathbb{R}^n \to \mathbb{R}^n$ is a continuous function of $\boldsymbol{x}$ with the usual assumptions that guarantee the existence and uniqueness of solutions of (1).

Assume that (1) may be separated in the following way:

$$\dot{\boldsymbol{y}} = \boldsymbol{f}_1(\boldsymbol{y}, \boldsymbol{z}, t), \tag{2a}$$
$$\dot{\boldsymbol{z}} = \boldsymbol{f}_2(\boldsymbol{y}, \boldsymbol{z}, t), \tag{2b}$$

with $\boldsymbol{y} \in \mathbb{R}^m$, $\boldsymbol{z} \in \mathbb{R}^p$, which form the vector $\boldsymbol{x}^T = [y_1, y_2, \ldots, y_m, z_1, z_2, \ldots, z_p]$; that is, $n = m + p$. The function $\boldsymbol{f}_1$ is assumed to satisfy $\boldsymbol{f}_1(0, \boldsymbol{z}, t) = 0$ for every $\boldsymbol{z}$ and t. Both $\boldsymbol{f}_1$ and $\boldsymbol{f}_2$ are assumed to be locally Lipschitz with respect to their arguments. Let $\boldsymbol{y}(t)$ and $\boldsymbol{z}(t)$ be solutions for the $\boldsymbol{y}$ and $\boldsymbol{z}$ dynamics, respectively; the initial conditions are denoted as $\boldsymbol{y}_0 = \boldsymbol{y}(0)$, $\boldsymbol{z}_0 = \boldsymbol{z}(0)$.

The study of partial stability theory provides a way to ensure that the $\boldsymbol{y}$ dynamics exhibit a certain behavior, which may be bounded or converge asymptotically, regardless of the behavior of solutions of $\boldsymbol{z}$. This is useful for cases where the dynamics of $\boldsymbol{y}$ are the main interest of the analysis. A comprehensive review of partial stability theory can be found in the works of Haddad and Chellaboina (2008) or Vorotnikov (1998).

A key concept in the study of partial stability is that of the continuation of solutions. A solution of (1) is continuable if the solution $\boldsymbol{x}(t)$ is defined for all $t \in \mathbb{R}_+$. A solution is forward complete if the same holds only for $t \geq 0$.

A major drawback when working with partial stability theorems is that it is always required to show that solutions are continuable or forward complete. This is not always a trivial task.

To continue the discussion of partial stability, consider the following definitions (Haddad and Chellaboina, 2008).

Definition 1. The nonlinear dynamical system (2a)–(2b) is Lyapunov stable with respect to $\boldsymbol{y}$ uniformly in $\boldsymbol{z}_0$ if, for every $\varepsilon > 0$, there exists $\mu = \mu(\varepsilon) > 0$ such that $\|\boldsymbol{y}_0\| < \mu$ implies that $\|\boldsymbol{y}(t)\| < \varepsilon$ for all $t \geq 0$ and for all $\boldsymbol{z}_0 \in \mathbb{R}^p$.

Definition 2. The nonlinear dynamical system (2a)–(2b) is asymptotically stable with respect to $\boldsymbol{y}$ uniformly in $\boldsymbol{z}_0$ if it is Lyapunov stable with respect to $\boldsymbol{y}$ uniformly in $\boldsymbol{z}_0$ and there exists $\mu > 0$ such that $\|\boldsymbol{y}_0\| < \mu$ implies that $\lim_{t\to\infty} \boldsymbol{y}(t) = 0$ uniformly in $\boldsymbol{y}_0$ and $\boldsymbol{z}_0$ for all $\boldsymbol{z}_0 \in \mathbb{R}^p$.

Global asymptotic stability with respect to $\boldsymbol{y}$ uniformly in $\boldsymbol{z}_0$ is attained if Definition 2 holds for any initial condition.

It is possible to show that the system (2a)–(2b) is asymptotically stable with respect to $\boldsymbol{y}$ uniformly in $\boldsymbol{z}_0$, i.e., $\lim\limits_{t\to\infty} \boldsymbol{y}(t) = \boldsymbol{0}$, with a convergence rate independent of the initial condition of the variable $\boldsymbol{z}$ by using the following theorem adapted from the one stated by Haddad and Chellaboina (2008).

Theorem 1. *Assume that solutions for (2a)–(2b) are forward complete. If there exist a continuously differentiable function $V : \mathbb{R}^m \times \mathbb{R}^p \times \mathbb{R}_+ \to \mathbb{R}$ and class $\mathcal{K}$ functions $\alpha(\cdot), \beta(\cdot), \gamma(\cdot)$ satisfying*

$$\alpha\left(\|\boldsymbol{y}\|\right) \leq V\left(\boldsymbol{y}, \boldsymbol{z}, t\right) \leq \beta\left(\|\boldsymbol{y}\|\right) \tag{3}$$

and

$$\dot{V}\left(\boldsymbol{y}, \boldsymbol{z}, t\right) \leq -\gamma\left(\|\boldsymbol{y}\|\right), \tag{4}$$

then the nonlinear dynamical system given by (2a)–(2b) is asymptotically stable with respect to $\boldsymbol{y}$ uniformly in $\boldsymbol{z}_0$.

If the functions $\alpha(\cdot), \beta(\cdot), \gamma(\cdot)$ are of class $\mathcal{K}_\infty$, global asymptotic stability with respect to $\boldsymbol{y}$ uniformly in $\boldsymbol{z}_0$ may be concluded.

As can be seen, this result, as many others, is based on the assumption of forward completeness. The problem of forward completeness can be made trivial provided that the system has a particular form and there exists a function V that satisfies the inequalities given in Theorem 1.

Consider, now, that the $\boldsymbol{z}$ dynamics are only a function of $\boldsymbol{y}$ as follows:

$$\dot{\boldsymbol{y}} = \boldsymbol{f}_1(\boldsymbol{y}, \boldsymbol{z}, t), \tag{5a}$$
$$\dot{\boldsymbol{z}} = \boldsymbol{f}_2(\boldsymbol{y}, t), \tag{5b}$$

where $\boldsymbol{f_2}$ is assumed to be uniformly bounded for bounded values of $\boldsymbol{y}$. That is, let $\mathcal{D} \subset \mathbb{R}^m$ be a compact subset of $\mathbb{R}^m$; then, there exists $k > 0$ such that for all $\boldsymbol{y} \in \mathcal{D}$, $\|\boldsymbol{f}_2(\boldsymbol{y}, t)\| \leq k$.

Systems in the form (5) are of great practical interest since many applications, such as output feedback and adaptive controllers, have this structure. Next, a new lemma is stated that will aid in proving the main result.

Lemma 1. *Assume that $\boldsymbol{f}_2$ in (5a)–(5b) is uniformly bounded for bounded values of $\boldsymbol{y}$. Let $V : \mathbb{R}^m \times \mathbb{R}^p \times \mathbb{R}_+ \to \mathbb{R}$ be a continuously differentiable function and $\alpha(\cdot), \beta(\cdot), \gamma(\cdot)$ be class $\mathcal{K}$ functions that satisfy*

$$\alpha\left(\|\boldsymbol{y}\|\right) \leq V\left(\boldsymbol{y}, \boldsymbol{z}, t\right) \leq \beta\left(\|\boldsymbol{y}\|\right) \tag{6}$$

and

$$\dot{V}\left(\boldsymbol{y}, \boldsymbol{z}, t\right) \leq -\gamma\left(\|\boldsymbol{y}\|\right). \tag{7}$$

Then the nonlinear dynamical system given by (5a)–(5b) are asymptotically stable with respect to $\boldsymbol{y}$ uniformly in $\boldsymbol{z}_0$.

Proof. By Theorem 1, (5a)–(5b) are asymptotically stable with respect to $\boldsymbol{y}$ uniformly in $\boldsymbol{z}_0$ provided that solutions are forward complete. To establish the forward completeness of the solutions, notice that, from the assumption that the system satisfies a local Lipschitz condition, a solution may be guaranteed to exist locally over a finite time interval $[0, t_1)$, with $0 < t_1 < \infty$. Over the interval of existence, from Definitions (1) and (2), and the existence of the function V, there exists a constant μ such that $\|\boldsymbol{y}_0\| < \mu$ implies $\|\boldsymbol{y}(t)\| < \varepsilon$. Consider now a number τ that satisfies $0 < \tau < t_1$. Then, any solution $\boldsymbol{z}(t)$ must satisfy

$$\boldsymbol{z}(\tau) - \boldsymbol{z}_0 \quad = \quad \int_0^\tau \boldsymbol{f}_2(\boldsymbol{y}, t)dt, \tag{8}$$

where integration of the vector is carried out in an element-wise fashion.

By the uniform boundedness of $\boldsymbol{f}_2$ and since $\|\boldsymbol{y}(t)\| < \varepsilon$, it is possible to see that

$$\|\boldsymbol{z}(\tau)\| \leq k\tau + \|\boldsymbol{z}_0\|. \tag{9}$$

Therefore, as $\tau \to t_1$, it is clear that $\boldsymbol{z}(\tau)$ remains bounded, which implies that the right limit exists and the solution may be continued to the right. The arbitrariness of t_1 proves the lemma. ■

Notice the fact that Lemma 1 replaces the requirement of forward completeness with that of uniform boundedness for the class of systems given by (5a)–(5b). This is far easier to show, which renders the result useful in practice.

3. Dynamical model of the BLDC motor

In this section, the mathematical model for the BLDC motor that will be used throughout the paper is presented. The equations that describe the behavior of the BLDC motor are deduced by Chiasson (2005). It is assumed that the stator windings are uniformly distributed throughout the surface of the stator and that the three-phase system is balanced. This implies that the magnetic fields are uniformly distributed. With the given assumptions, the model may be expressed as

$$\mathbf{L}\frac{d}{dt}\mathbf{i}_s = E_p\omega\mathbf{E}_R\left(\theta\right) - \mathbf{R}_s\mathbf{i}_s + \boldsymbol{v}_s, \tag{10a}$$

$$J\frac{d}{dt}\omega = -\tau_p\mathbf{E}_R^T\left(\theta\right)\mathbf{i}_s - B\omega - \tau_L, \tag{10b}$$

where $\boldsymbol{v}_s = \left[v_{s_1}\, v_{s_2}\, v_{s_3}\right]^T \in \mathbb{R}^3$ denotes the stator supply voltages while $\mathbf{i}_s = \left[i_{s_1}\, i_{s_2}\, i_{s_3}\right]^T \in \mathbb{R}^3$ are the stator currents, $\theta \in \mathbb{R}$ represents the angular position of the rotor and ω its angular velocity. The parameters J and B denote the moment of inertia of the rotor and the viscous friction coefficient, respectively, and τ_L is used to represent an external load applied to the shaft of the motor.

By assuming that the rotor is surface-mounted, it can be stated that the rotor does not have any saliency. Therefore, the inductance matrix $\mathbf{L} \in \mathbb{R}^{3\times3}$ is a constant positive definite matrix given by

$$\mathbf{L} = \begin{bmatrix} L_s & -M & -M \\ -M & L_s & -M \\ -M & -M & L_s \end{bmatrix}, \tag{11}$$

where L_s is the self-inductance of the windings of the stator and M is the mutual inductance (also called dispersion inductance) of the phases. From the physical structure of the machine, it holds that $L_s = (7/3)M$ (Chiasson, 2005, p. 661).

The matrix $\mathbf{R}_s = R_s\mathbf{I}_3 \in \mathbb{R}^{3x3}$ is used to represent the stator resistance one. The constant R_s denotes the phase windings' resistances, which can be assumed to be equal without loss of generality.

The parameter E_p relates the density of the magnetic field of the permanent magnet with the number of turns in the windings and their length. It is commonly referred to as the back-EMF constant. The parameter τ_p, known as the torque constant, serves the same purpose as E_p. Even though their value is equal, that is, $E_p = \tau_p$, it is due to convention that two different symbols are used to identify them.

The vector $\mathbf{E}_R\left(\theta\right) = \begin{bmatrix} E_1\left(\theta\right) & E_2\left(\theta\right) & E_3\left(\theta\right) \end{bmatrix}^T \in \mathbb{R}^3$ has as elements three periodic trapezoidal functions that are out of phase with each other by $(2/3)\pi$ rad, i.e.,

$$\mathbf{E}_R\left(\theta\right) = \begin{bmatrix} E\left(\theta\right) & E\left(\theta - \frac{2}{3}\pi\right) & E\left(\theta + \frac{2}{3}\pi\right) \end{bmatrix}^T. \tag{12}$$

Over one period of the periodic trapezoidal function,

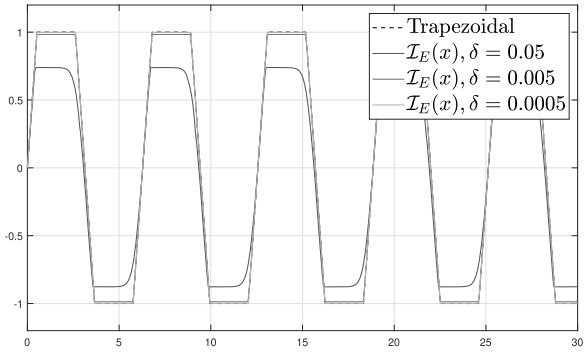

(a) trapezoidal and approximation $\mathcal{I}_E$.

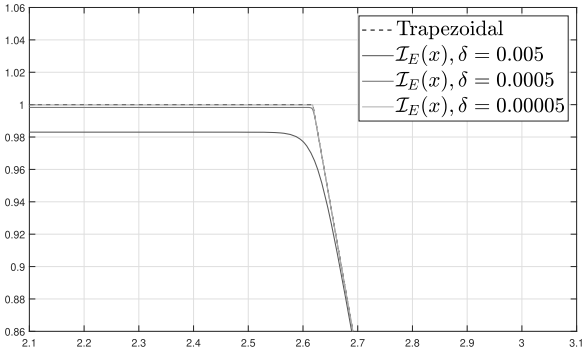

(b) close-up view of the approximation.

Fig. 1. Comparison of the trapezoidal function and approximation for different values of δ.

the values of $E(\theta)$ are defined as

$$E(\theta) = \begin{cases} \dfrac{6\theta}{\pi}, & -\dfrac{\pi}{6} \leq \theta \leq \dfrac{\pi}{6}, \\ 1, & \dfrac{\pi}{6} \leq \theta \leq \dfrac{5\pi}{6}, \\ -\dfrac{6(\theta-\pi)}{\pi}, & \dfrac{5\pi}{6} \leq \theta \leq \dfrac{7\pi}{6}, \\ -1, & \dfrac{7\pi}{6} \leq \theta \leq \dfrac{11\pi}{6}. \end{cases} \tag{13}$$

3.1. Approximation of $\mathbf{E_R}$ via the integral of a smooth window-like wave. The vector $\mathbf{E}_R$ is not differentiable at some points, so this leads to a more complex theoretical stability analysis since the closed loop equation does not satisfy the usual existence and uniqueness theorems. Nevertheless, in order to solve the above mentioned problem, in this work, a novel differentiable approximation is introduced, and can be constructed for the non-differentiable function (12) in the following way. Let

$$\bar{\mathbf{E}}_R(\theta) = \begin{bmatrix} \bar{E}_1(\theta) & \bar{E}_2(\theta) & \bar{E}_3(\theta) \end{bmatrix}^T \tag{14}$$

denote the approximation of $\mathbf{E}_R$.

An approximation of the trapezoidal function can be constructed by taking the integral of a smooth window-like function. To specify the function, several others will be defined first. To this end, let $1 > \delta > 0$ be a positive number and consider the following definitions:

$$\Omega_T(q) = \frac{2}{\pi(1-\delta)} \sin^{-1}((1-\delta)\sin(q)), \tag{15a}$$

$$\Omega_{SQ}(q) = \tanh\left(\frac{\sin(q)}{\delta}\right). \tag{15b}$$

The shape of Ω_T bears a resemblance to a smooth triangular wave and Ω_{SQ} resembles a smooth square wave. Notice that both functions are periodic and differentiable over the whole domain $\mathbb{R}$. By using the definitions presented in (15a) and (15b), it is possible to construct a smooth saw tooth-like function in the following way:

$$\Omega_{SW}(q) = \frac{1}{2}\left\{\Omega_T(2q)\Omega_{SQ}\left(2q + \frac{\pi}{2}\right) + 1\right\}. \tag{16}$$

Now, the smooth periodic window-like function can be denoted as

$$\mathcal{W}(q) = \frac{1}{2}\left\{\tanh\left(\frac{1}{\delta}\left[\Omega_{SW}\left(\frac{q}{4} - \frac{\pi}{24}\right) - \frac{5}{6}\right]\right) + 1\right\}. \tag{17}$$

This allows forming the definition of a continuous vector function $\mathbf{E}_R^* = \begin{bmatrix} E_1^*(\theta) & E_2^*(\theta) & E_3^*(\theta) \end{bmatrix}^T$, which denotes the derivative of the approximation and is given by

$$\mathbf{E}_R^*(\theta) = \begin{bmatrix} \mathcal{W}_E(\theta) & \mathcal{W}_E\left(\theta - \frac{2}{3}\pi\right) & \mathcal{W}_E\left(\theta + \frac{2}{3}\pi\right) \end{bmatrix}^T, \tag{18}$$

with the function $\mathcal{W}_E$ given by

$$\mathcal{W}_E(q) = \frac{6}{\pi}(\mathcal{W}(q-\pi) - \mathcal{W}(q)). \tag{19}$$

Finally, the trapezoidal approximation is constructed as

$$\bar{\mathbf{E}}_R(\theta) = \begin{bmatrix} \mathcal{I}_E(\theta) & \mathcal{I}_E\left(\theta - \frac{2}{3}\pi\right) & \mathcal{I}_E\left(\theta + \frac{2}{3}\pi\right) \end{bmatrix}^T, \tag{20}$$

where $\mathcal{I}_E$ is a function given by

$$\mathcal{I}_E(q) = \int_0^q \mathcal{W}_E(\sigma)d\sigma. \tag{21}$$

The functions expressed in (20) are approximations to the trapezoidal functions (12) that are used in the mathematical model of the BLDC motor. The functions (20) can be used in the design of the proposed control strategy, as well as their derivative with respect to time. The time derivative of (21) is

$$\frac{d}{dt}\left(\mathcal{I}_E(\theta)\right) = \dot{\theta}\mathcal{W}_E(\theta). \tag{22}$$

The time derivative of the inner product of (20) is

$$\frac{d}{dt}\left\|\bar{\mathbf{E}}_R(\theta)\right\|^2 = 2\dot{\theta}\left(\mathbf{E}_R^*(\theta)\right)^T\bar{\mathbf{E}}_R(\theta). \tag{23}$$

The proposed approximation function is shown in Fig. 1. Figure 1(a) presents the approximation for several values of δ, and it can be seen that smaller values of δ improve the approximation. Figure 1(b) is the close-up view of the upper right corner of the approximation.

The time derivative of the approximation function (19) for different values of δ is shown in Fig. 2.

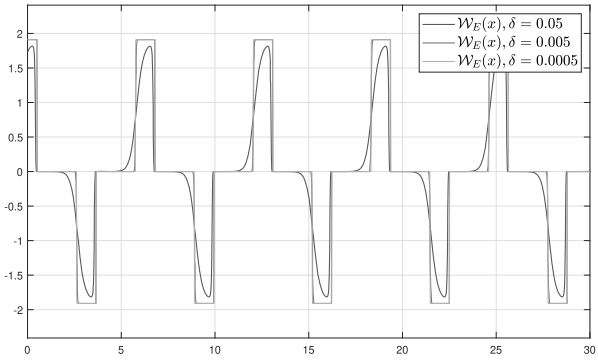

Fig. 2. Derivative $\mathcal{W}_E$ of the approximation for different values of δ.

4. Control law design

This section presents a control law design that guarantees that the desired velocity objective is met without velocity measurements in the sense described in the problem statement section.

4.1. Problem statement. Let $\omega_d(t)$ denote the desired angular velocity of the rotor. The control objective will be to achieve the asymptotic tracking of the specified angular velocity on a BLDC motor without velocity feedback. In other words, the control law must be designed such that

$$\lim_{t\to\infty}|\omega(t)-\omega_d(t)| = 0 \tag{24}$$

without using velocity measurements. The feedback is composed solely by the stator currents and the position measurement of the rotor.

To fulfill (24), the control law is applied through the control inputs, which are the voltages applied to the stator windings denoted as $\boldsymbol{v}_s$ (see Fig. 3). Additionally, to solve the control problem, the following assumptions are introduced:

S.1. The mathematical model of a BLDC motor is given by (10a)–(10b).

S.2. The stator currents $\mathbf{i}_s$ and the angular position of the rotor θ are available for measurement.

S.3. The mechanical and electrical parameters of the BLDC motor are known.

S.4. The desired angular velocity ω_d is a continuous function of time. By design, it is a twice differentiable function.

S.5 The load torque τ_L is a known differentiable function of time.

4.2. Controller design. First, consider a second-order filter given by a second-order transfer function with two repeated real poles and one zero. Due to the difference in degrees of the denominator polynomial and that of the numerator polynomial, this transfer function is of relative degree 1, so it is strictly proper (Ioannou and Sun, 1996), and its state-space representation is

$$\begin{bmatrix}\dot{x}_{1f}\\ \dot{x}_{2f}\end{bmatrix} = \begin{bmatrix}0 & 1\\ -\lambda_d^2 & -2\lambda_d\end{bmatrix}\begin{bmatrix}x_{1f}\\ x_{2f}\end{bmatrix} + \begin{bmatrix}0\\ \lambda_d^2\end{bmatrix}e_\theta, \tag{25}$$

where $\lambda_d > 0$ is a constant and $e_\theta(t)$ is the input to system given by $e_\theta(t) = \theta_d - \theta$, with θ_d denoting the integral of the desired velocity, that is, $\theta_d = \int_0^t \omega_d(\sigma)d\sigma$.

Let the desired stator currents $\mathbf{i}_{s_d} \in \mathbb{R}^3$ be defined as

$$\mathbf{i}_{s_d} = \frac{1}{E_p}\frac{(-\tau_L - J\dot{\omega}_d - B\omega_d + K_\vartheta\vartheta)}{\left\|\bar{\mathbf{E}}_R(\theta)\right\|^2}\bar{\mathbf{E}}_R(\theta), \tag{26}$$

where $K_\vartheta > 0$ is a constant while ϑ denotes a linear combination of the states of the filter (25) and the position error in the following way:

$$\vartheta = \frac{1}{\lambda_d}(x_{2f} + \lambda_d x_{1f} - \lambda_d e_\theta). \tag{27}$$

The time derivative of ϑ may be expressed as

$$\dot{\vartheta} = -\left(\lambda_d\vartheta + \dot{e}_\theta\right). \tag{28}$$

The control law, which is the voltage $\boldsymbol{v}_s$ applied at the stator of the BLDC motor, is specified to be

$$\begin{aligned}\boldsymbol{v}_s = {}& \mathbf{L}\frac{d}{dt}\mathbf{i}_{s_{da}} + \mathbf{R}_s\mathbf{i}_{s_d} - E_p\bar{\mathbf{E}}_R(\theta)\omega_d + K_e\mathbf{e}_I\\ & + x_{2f}\mathbf{L}\boldsymbol{\Delta}_i,\end{aligned} \tag{29}$$

where $K_e > 0$ is a constant. The term $\frac{d}{dt}\mathbf{i}_{s_{da}}$ is given by the expression

$$\frac{d}{dt}\mathbf{i}_{s_{da}} = \boldsymbol{\Upsilon}\frac{\alpha_1}{\beta}(\omega_d - x_{2f}) + \frac{\dot{\alpha}_1}{\beta}\bar{\mathbf{E}}_R(\theta) \tag{30}$$

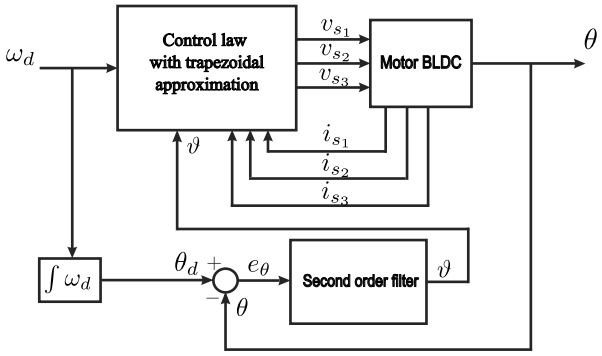

Fig. 3. Closed loop control scheme.

with

$$\boldsymbol{\Upsilon} = \left[\mathbf{E}_R^* (\theta) - \frac{2\bar{\mathbf{E}}_R^T (\theta)\, \mathbf{E}_R^*}{\left\| \bar{\mathbf{E}}_R (\theta) \right\|^2} \bar{\mathbf{E}}_R (\theta) \right],$$

and $\boldsymbol{\Delta}_i$ is defined as

$$\boldsymbol{\Delta}_i = \boldsymbol{\Upsilon} \frac{\alpha_1}{\beta} + \frac{K_\vartheta}{\beta} \bar{\mathbf{E}}_R (\theta) \tag{31}$$

whilst α_1, $\dot{\bar{\alpha}}_1$ and β as

$$\alpha_1 = -\tau_L - J\dot{\omega}_d - B\omega_d + K_\vartheta \vartheta, \tag{32a}$$

$$\dot{\bar{\alpha}}_1 = -\dot{\tau}_L - J\ddot{\omega}_d - B\dot{\omega}_d - K_\vartheta \vartheta - x_{2f} K_\vartheta, \tag{32b}$$

$$\beta = E_p \left\| \bar{\mathbf{E}}_R (\theta) \right\|^2. \tag{32c}$$

As was seen in the previous section, the vector $\mathbf{E}_R^*$ represents the derivative of $\bar{\mathbf{E}}_R(\theta)$ with respect to θ. $\bar{\mathbf{E}}_R(\theta)$ is the differentiable approximation of the non-differentiable trapezoidal function. The approximation $\bar{\mathbf{E}}_R$ is assumed to be equal to the model. This is equivalent to the practical assumption that the difference between the approximate model and the real one is negligible.

Figure 3 shows the block diagram of the closed-loop control scheme.

4.3. Closed-loop dynamics. Consider the mathematical model of the BLDC motor as given by (10a)–(10b). Let $\mathbf{x} = \begin{bmatrix} \mathbf{i}_s & \omega \end{bmatrix}^T \in \mathbb{R}^4$ denote the vector of states and $\boldsymbol{Q} = \begin{bmatrix} \boldsymbol{v}_s & -\tau_L \end{bmatrix}^T \in \mathbb{R}^4$ a vector that denotes external inputs.

It is possible to rewrite (10a)–(10b) as

$$\boldsymbol{\mathcal{D}} \dot{\mathbf{x}} + \boldsymbol{\mathcal{R}} \mathbf{x} + \bar{\boldsymbol{\mathcal{C}}} (\theta)\, \mathbf{x} = \boldsymbol{Q}, \tag{33}$$

with $\boldsymbol{\mathcal{D}} \in \mathbb{R}^{4\times4}$, $\boldsymbol{\mathcal{R}} \in \mathbb{R}^{4\times4}$ and $\bar{\boldsymbol{\mathcal{C}}} (\theta) \in \mathbb{R}^{4\times4}$ defined as

$$\boldsymbol{\mathcal{D}} = \begin{bmatrix} \mathbf{L} & \mathbf{0}_{3x1} \\ \mathbf{0}_{1x3} & J \end{bmatrix}, \qquad \boldsymbol{\mathcal{R}} = \begin{bmatrix} \mathbf{R}_s & \mathbf{0}_{3x1} \\ \mathbf{0}_{1x3} & B \end{bmatrix}, \tag{34a}$$

$$\bar{\boldsymbol{\mathcal{C}}} (\theta) = \begin{bmatrix} \mathbf{0}_{3x3} & -E_p \bar{\mathbf{E}}_R (\theta) \\ E_p \bar{\mathbf{E}}_R^T (\theta) & 0 \end{bmatrix}. \tag{34b}$$

In the matrix $\bar{\boldsymbol{\mathcal{C}}} (\theta)$ the trapezoidal approximation $\bar{\mathbf{E}}_R (\theta)$, defined in (20), was used.

The elements of the vector $\mathbf{x}$ may be related to their desired values $\mathbf{x}_d$ by defining an error vector $\mathbf{e} = \begin{bmatrix} \mathbf{e}_I & e_\omega \end{bmatrix}^T \in \mathbb{R}^4$ as

$$\mathbf{e} = \mathbf{x}_d - \mathbf{x}, \tag{35}$$

with $\mathbf{e}_I = \mathbf{i}_{sd} - \mathbf{i}_s$ and $e_\omega = \omega_d - \omega$

The error vector defined in (35) allows providing restatement of (33) in terms of the error vector $\mathbf{e}$. To this end, notice that (33) may be written as

$$\boldsymbol{\mathcal{D}} \dot{\mathbf{e}} + \boldsymbol{\mathcal{R}} \mathbf{e} + \bar{\boldsymbol{\mathcal{C}}} (\theta)\, \mathbf{e} = \boldsymbol{\Psi}, \tag{36}$$

where the function $\boldsymbol{\Psi} \in \mathbb{R}^{4\times4}$ denotes the vector

$$\boldsymbol{\Psi} = -\boldsymbol{Q} + \boldsymbol{\mathcal{D}} \dot{\mathbf{x}}_d + \boldsymbol{\mathcal{R}} \mathbf{x}_d + \bar{\boldsymbol{\mathcal{C}}} (\theta)\, \mathbf{x}_d. \tag{37}$$

The structure of the vector (37) can be seen to be composed of three elements associated to the electrical dynamics $\boldsymbol{\Psi}_e$ and one associated to the mechanical subsystem Ψ_m. The elements that correspond to the electrical dynamics are given by

$$\boldsymbol{\Psi}_e = -\mathbf{v}_s + \mathbf{L} \frac{d}{dt} \mathbf{i}_{sd} + \mathbf{R}_s \mathbf{i}_{sd} - E_p \bar{\mathbf{E}}_R (\theta)\, \omega_d, \tag{38}$$

and the element corresponding to the mechanical subsystem is given by

$$\Psi_m = \tau_L + J \frac{d}{dt} \omega_d + B\omega_d + E_p \bar{\mathbf{E}}_R^T (\theta)\, \mathbf{i}_{sd}. \tag{39}$$

By substituting (26) into (39), Ψ_m reduces to

$$\Psi_m = K_\vartheta \vartheta. \tag{40}$$

In a similar manner, by replacing (29) in (38) it holds that

$$\boldsymbol{\Psi}_e = -K_e \mathbf{e}_I + \mathbf{L} \left(\frac{d}{dt} \mathbf{i}_{sd} - \frac{d}{dt} \mathbf{i}_{sda} \right) - x_{2f} \mathbf{L} \boldsymbol{\Delta}_i. \tag{41}$$

The derivative of the desired currents $\mathbf{i}_{sd}$ given in (26) may be computed as

$$\frac{d}{dt} \mathbf{i}_{sd} = \boldsymbol{\Upsilon} \frac{\alpha_1}{\beta} \omega + \frac{\dot{\alpha}_1}{\beta} \bar{\mathbf{E}}_R (\theta), \tag{42}$$

with the functions α_1 and β defined in (32).

By using (30), Eqn. (41) can be simplified by noting that

$$\frac{d}{dt} \mathbf{i}_{sd} - \frac{d}{dt} \mathbf{i}_{sda} = \boldsymbol{\Delta}_i \left[x_{2f} - e_\omega \right]. \tag{43}$$

Consequently, $\boldsymbol{\Psi}_e$ can be expressed as

$$\boldsymbol{\Psi}_e = -K_e \mathbf{e}_I - \mathbf{L} \boldsymbol{\Delta}_i e_\omega. \tag{44}$$

Therefore, from (40) and (44), the function (37) can be expressed as

$$\boldsymbol{\Psi} = \begin{bmatrix} -K_e \mathbf{e}_I - \mathbf{L}\boldsymbol{\Delta}_i e_\omega \\ K_\vartheta \vartheta \end{bmatrix}. \tag{45}$$

Using (45), the closed-loop system (36) can be written as

$$\mathbf{L}\dot{\mathbf{e}}_I = \left(E_p \bar{\mathbf{E}}_R(\theta) - \mathbf{L}\boldsymbol{\Delta}_i\right) e_\omega - \left(\mathbf{R}_s + K_e \mathbf{I}_3\right) \mathbf{e}_I, \tag{46a}$$

$$J\dot{e}_\omega = -B e_\omega - E_p \bar{\mathbf{E}}_R^T(\theta)\, \mathbf{e}_I + K_\vartheta \vartheta. \tag{46b}$$

The system given in (46) can be written in compact form as

$$\boldsymbol{\mathcal{D}}\dot{\mathbf{e}} = -\bar{\boldsymbol{\mathcal{R}}}\mathbf{e} - \bar{\boldsymbol{\mathcal{C}}}(\theta)\, \mathbf{e} + \boldsymbol{\delta}, \tag{47}$$

with the matrix $\bar{\boldsymbol{\mathcal{C}}}$ given in (34b) and the matrices $\bar{\boldsymbol{\mathcal{R}}}$ and $\boldsymbol{\delta}$ structured as

$$\bar{\boldsymbol{\mathcal{R}}} = \begin{bmatrix} (\mathbf{R}_s + K_e \mathbf{I}_3) & \mathbf{0}_{3x1} \\ \mathbf{0}_{1x3} & B \end{bmatrix}, \tag{48a}$$

$$\boldsymbol{\delta} = \begin{bmatrix} -\mathbf{L}\boldsymbol{\Delta}_i e_\omega \\ K_\vartheta \vartheta \end{bmatrix}. \tag{48b}$$

The complete closed-loop system is conformed by (46a) and (46b), and (25) has as states $\mathbf{e}_I$, e_ω, e_θ, as well as x_{1f} and x_{2f} with the extra state ϑ.

4.4. Stability analysis. Consider the function

$$\mathcal{H}_e = \frac{1}{2}\mathbf{e}^T \boldsymbol{\mathcal{D}} \mathbf{e} + \frac{1}{2} K_\vartheta \vartheta^2. \tag{49}$$

The function (49) is positive definite since the matrix $\boldsymbol{\mathcal{D}}$, given in (34a), is positive definite according to the assumption S.3 and the constant $K_\vartheta > 0$.

By defining the vector $\boldsymbol{y} = [\mathbf{e} \quad \vartheta]^T$, it is possible to see that there exist constants $h_{\max}, h_{\min} > 0$ such that $h_{\min}\|\boldsymbol{y}\|^2 \leq \mathcal{H}_e \leq h_{\max}\|\boldsymbol{y}\|^2$.

For some positive constant c, the set $\Gamma = \{\boldsymbol{y} \in \mathbb{R}^5 : \|\boldsymbol{y}\|^2 < c\}$ is non-compact over the whole state space. However, it is bounded in the direction of the elements used to define $\boldsymbol{y}$.

The time derivative of (49) is

$$\dot{\mathcal{H}}_e = \mathbf{e}^T \boldsymbol{\mathcal{D}} \dot{\mathbf{e}} + K_\vartheta \vartheta \dot{\vartheta}. \tag{50}$$

From (28) and the closed-loop equations (46a), (46b) and (25), it is possible to rewrite (50) as

$$\dot{\mathcal{H}}_e = \mathbf{e}^T \left(-\bar{\boldsymbol{\mathcal{R}}}\mathbf{e} - \bar{\boldsymbol{\mathcal{C}}}(\theta)\, \mathbf{e} + \boldsymbol{\delta}\right) - K_\vartheta \lambda_d \vartheta^2 - K_\vartheta \vartheta e_\omega. \tag{51}$$

Since $\bar{\boldsymbol{\mathcal{C}}}$ is an antisymmetric matrix, and from the definition of $\boldsymbol{\delta}$, it holds that

$$\dot{\mathcal{H}}_e = -\mathbf{e}^T \bar{\boldsymbol{\mathcal{R}}} \mathbf{e} - K_\vartheta \lambda_d \vartheta^2 - \mathbf{e}_I^T \mathbf{L}\boldsymbol{\Delta}_i e_\omega. \tag{52}$$

Now notice that there exist constants $k_{\Delta 1}, k_{\Delta 2} > 0$ such that

$$\|\mathbf{L}\boldsymbol{\Delta}_i\| \leq K_\vartheta (k_{\Delta 1}|\vartheta| + k_{\Delta 2}), \tag{53}$$

given by

$$k'_{\Delta 1} \triangleq \max_{\theta \in \mathbb{R}} \left\{ \|\boldsymbol{\Upsilon}\| \frac{1}{\beta} \right\}, \tag{54}$$

$$k'_{\Delta 2} \triangleq \max_{\theta \in \mathbb{R}} \left\{ \frac{1}{\beta} \|\bar{\mathbf{E}}_R\| \right\} + \max_{t,\theta \in \mathbb{R}} \left\{ \|\boldsymbol{\Upsilon}\| \frac{|-\tau_L - J\dot{\omega}_d - B\omega_d|}{K_\vartheta \beta} \right\}, \tag{55}$$

$$k_{\Delta 1} \triangleq \max_{\theta \in \mathbb{R}} \{\mathbf{L}\}\, k'_{\Delta 1}, \tag{56}$$

$$k_{\Delta_2} \triangleq \max_{\theta \in \mathbb{R}} \{\mathbf{L}\}\, k'_{\Delta 2}. \tag{57}$$

This implies that (52) can be upper bounded by

$$\dot{\mathcal{H}}_e \leq -(R_s + K_e)\|\mathbf{e}_I\|^2 - B|e_\omega|^2 - K_\vartheta \lambda_d |\vartheta|^2 + K_\vartheta (k_{\Delta 1}|\vartheta| + k_{\Delta 2})\|\mathbf{e}_I\||e_\omega|. \tag{58}$$

Now notice that, for any $\gamma_1 > 0$, the upper bound

$$K_\vartheta k_{\Delta 1}|\vartheta|\|\mathbf{e}_I\||e_\omega| \leq \frac{K_\vartheta k_{\Delta 1} c}{2\gamma_1}\|\mathbf{e}_I\|^2 + \frac{K_\vartheta k_{\Delta 1} c \gamma_1}{2}|e_\omega|^2 \tag{59}$$

holds on Γ. Similarly, for any $\gamma_2 > 0$,

$$K_\vartheta k_{\Delta 2}\|\mathbf{e}_I\||e_\omega| \leq \frac{K_\vartheta k_{\Delta 2}}{2\gamma_2}\|\mathbf{e}_I\|^2 + \frac{K_\vartheta k_{\Delta 2}\gamma_2}{2}|e_\omega|^2. \tag{60}$$

Therefore, (58) will be non-positive because it is possible to find suitable combinations of γ_1, γ_2, sufficiently small and K_e sufficiently large, which satisfy

$$-\beta + \frac{\gamma_1 K_\vartheta k_{\Delta 1} c}{2} + \frac{\gamma_2 K_\vartheta k_{\Delta 2}}{2} \leq 0, \tag{61}$$

$$K_\vartheta (k_{\Delta 1} c \gamma_2 + k_{\Delta 2}\gamma_1) - 2\gamma_1\gamma_2(R_s + K_e) \leq 0. \tag{62}$$

It holds that $\dot{\mathcal{H}}_e \leq -k_{\mathcal{H}}\|\boldsymbol{y}\|^2$ for $k_{\mathcal{H}} > 0$ given by

$$k_{\mathcal{H}} \triangleq \min \left\{ (R_s + K_e) - \frac{K_\vartheta k_{\Delta 1} c}{2\gamma 1} - \frac{K_\vartheta k_{\Delta 2}}{2\gamma 2}, \beta - \frac{\gamma_1 K_\vartheta k_{\Delta 1} c}{2} - \frac{\gamma_2 K_\vartheta k_{\Delta 2}}{2} \right\}, \tag{63}$$

which will be positive provided that (61) and (62) are satisfied.

Next, let $\boldsymbol{z} = [e_\theta]$. Then, by using Lemma 1, the system will be asymptotically stable with respect to $\boldsymbol{y}$ uniformly in $\boldsymbol{z}_0$, since $\dot{e}_\theta = e_\omega$ is uniformly bounded for bounded values of e_ω, if the solutions to the state equation x_{1_f} and x_{2_f} of the filter are forward complete. This can easily be seen to hold since the filter is input to state-stable with x_{1_f} and x_{2_f} as states and e_ω as input.

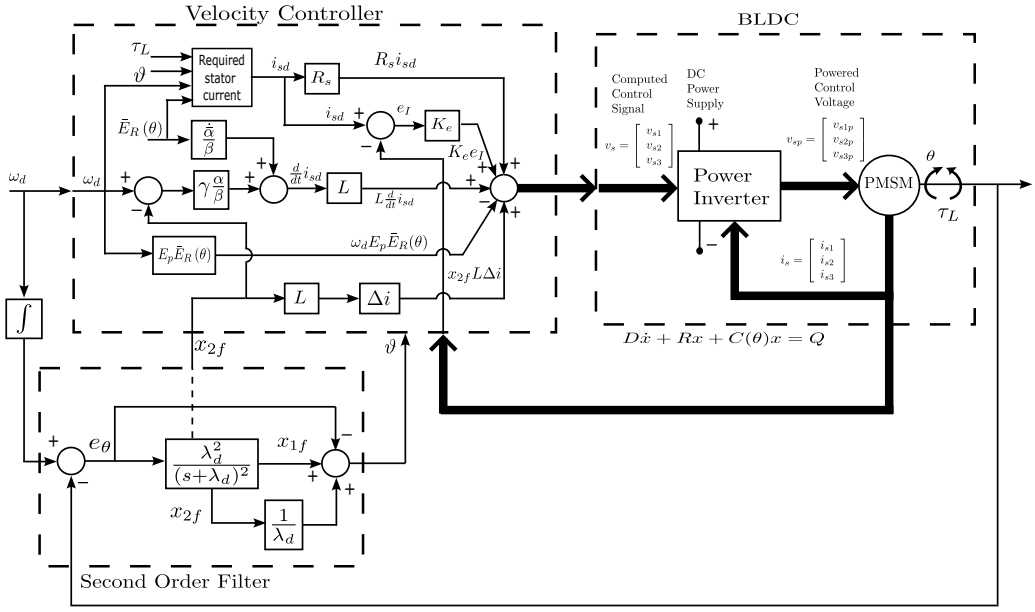

Fig. 4. Detailed block diagram of the control system.

This implies that there exists $\mu > 0$ such that $\|\boldsymbol{y}_0\| < \mu$ implies $\mathbf{e}_I \to 0$, $e_\omega \to 0$ and $\vartheta \to 0$ as $t \to \infty$ uniformly in $\boldsymbol{y}_0$ and any initial condition of the rest of the states. Consequently, the control objective is met.

Remark 1. The only condition on the gains of the controller is given by (62). The first element of the right hand side of the inequality implies that the region of attraction can be made bigger by increasing K_e since it depends on c. The constant c can be selected in practice by using the initial condition of the elements of $\boldsymbol{y}$. This follows from the fact that $\dot{\mathcal{H}}_e \leq 0$ implies $\mathcal{H}_e(\boldsymbol{y}(t)) \leq \mathcal{H}_e(\boldsymbol{y}_0)$. Therefore, c can be chosen such that $\mathcal{H}_e(\boldsymbol{y}_0) \leq c$. This also means that $\Gamma_{\mathcal{H}}$ is defined as the set where $\mathcal{H}_e \leq c$ is positively invariant, that is, $\Gamma_{\mathcal{H}}$ is an estimate of the region of attraction.

5. Simulation results

A simulation was constructed in order to validate the proposed control scheme. The BLDC motor model given by (10) was programmed together with the control scheme given by (26), (29), and (30) using the trapezoidal approximation defined in (20). The second-order filter was introduced using its state space representation (25). And SIMULINK/MATLAB® was employed to implement the simulation. The Dormand-Prince integration method was used with a fixed integration step of 0.01 ms. Figure 4 shows a detailed block diagram of the proposed BLDC motor control system.

The BLDC motor parameters that were used in the numerical simulation experiment are $R_s = 0.7\ \Omega$, $L_s = 0.0027$ H, $M = 0.0012$ H, $E_p = 0.5128$ Nm/A, $J = 0.0002$ kgm^2 and $B = 0.002$ Nms/rad. The parameters of the simulated motor were taken after Krishnan (2001) and Chiasson (2005). Those authors also define a maximum supply voltage (peak) of 200 V and a maximum current of 10 A. The actuation limits were never reached in the tests that were carried out.

The velocity reference that was used is given by

$$\omega_d = \begin{cases} 0, & 0 \leq t \leq t_0, \\ c_1(t-t_0)^2 + c_2(t-t_0)^3, & t_0 \leq t \leq t_1, \\ \omega_{\max}, & t_1 \leq t \leq t_2, \\ c_1(t_3-t)^2 + c_2(t_3-t)^3, & t_2 \leq t \leq t_3, \\ 0, & t_3 < t, \end{cases} \tag{64}$$

with $\omega_{\max} = 500$ rpm and the time intervals $t_0 = 1$ s, $t_1 = 11$ s, $t_2 = 21$ s and $t_3 = 31$ s. The constants c_1 and c_2 of (64) are calculated as

$$c_1 = \frac{3\omega_{\max}}{(t_1 - t_0)^2}, \tag{65a}$$

$$c_2 = -\frac{2\omega_{\max}}{(t_1 - t_0)^3}. \tag{65b}$$

The desired velocity function (64) was first used by Guerrero and Santibañez (2021) and satisfies the requirements of the assumption S.4, i.e., it is continuous and twice differentiable. In the whole system simulation, it is required to have the first and second time derivatives of the desired angular velocity (specifically, in the motor dynamical system, in the second order filter, and in the control law); these terms are obtained in an analytical way from (64) instead of using a Simulink derivative block.

The constants δ, λ_d, K_ϑ, and K_e, required in the controller, for stability analysis, must be positive. The

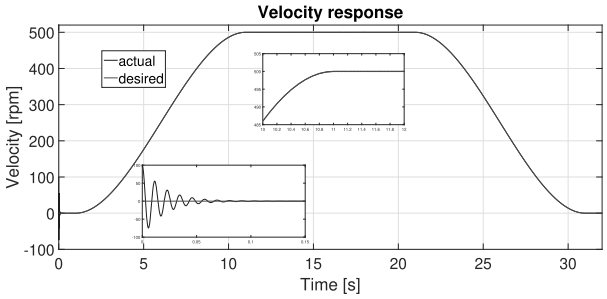

Fig. 5. Velocity response without a load torque.

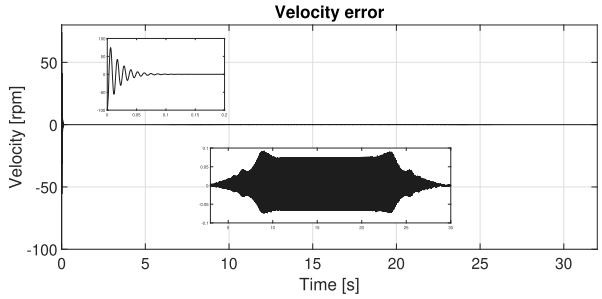

Fig. 6. Velocity error response without a load torque.

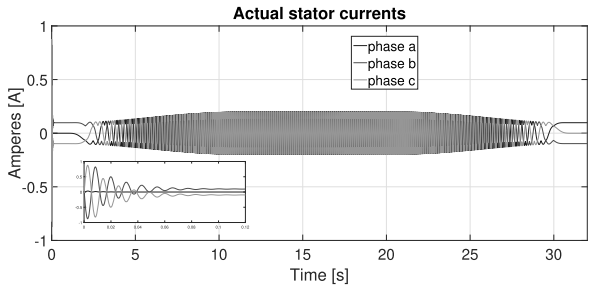

Fig. 7. Stator currents without a load torque.

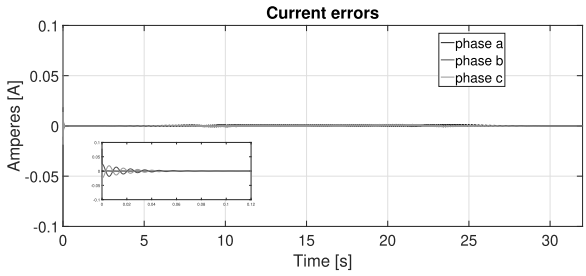

Fig. 8. Stator currents error without a load torque.

values of the proposed controller gains were chosen as $K_e = 120$, $K_\vartheta = 0.75$, $\lambda_d = 80$, and for the constant of trapezoidal approximation a value of $\delta = 0.000000000001$ was used.

With the intention of evaluating the performance of the control law, two numerical simulations are developed with the following scenarios: (i) first, angular velocity control is implemented considering a small constant load torque due to an encoder coupled to the shaft; (ii) the second simulation considers a load torque which emulates a clutch, that is, the load is applied and released at different points in time.

5.1. Without a load torque. As already mentioned, the first simulation considers a small constant torque load of 0.1 Nm emulating an encoder coupled to the shaft.

Figure 5 presents two plots, the desired velocities (in light gray) and the real unmeasured velocity (in dark gray) of the BLDC motor under the proposed control law and the aforementioned conditions considering an initial condition for the motor shaft velocity of 100 rpm. The figure shows that the desired angular velocity is tracked throughout the span of the simulation time. It can be seen, at the start of the simulation, that the lower left zoom box of the figure shows that the motor shaft velocity is 100 rpm, due to the initial condition. It exhibits an oscillatory response around 0 rpm before 0.1 s, and after this time, it has a steady-state response at zero, according to the reference velocity. The tracking of the angular velocity of the shaft to the desired one, can be seen in the zoom box at the top center in Fig. 5.

To evaluate the performance of the tracking controller, Fig. 6 shows the velocity error, and it can be seen in the zoom box at the top left that, at the beginning of the simulation, due to the fact of the assumption of the initial condition on the motor shaft, there is a difference of 100 rpm, tending the error to zero in approximately 0.1 s. Afterwards, it can be observed in the zoom box at the bottom center in the figure that the maximum velocity error is smaller than 0.1 rpm at two times: first, when the maximum velocity is reached (around 8.9 s); and then, when the velocity reference starts to decay (around 23.1 s). The error does not decay completely to zero since the integration scheme is discrete and the controller is designed using the differentiable approximation of trapezoidal functions, while the BLDC motor model is programmed using non-differentiable trapezoidal ones. Despite this difference, the velocity error is less than 0.02% when compared to the maximal value of the desired reference.

The current consumption of the stator windings is shown in Fig. 7. Here, it can be observed that, as the velocity reference increases, the currents have a quasi-trapezoidal shape and the frequency increases, with an amplitude of 0.2 A at the maximum velocity. Also, it can be noted that, when the desired angular velocity is equal to zero, the three stator currents are constants. The phase "a" is 0 A and the remaining two are equal to 0.1 A, due to the small load in the shaft. Due to the assumption of the initial condition of the motor shaft velocity, it can be seen in the zoom box at the bottom left

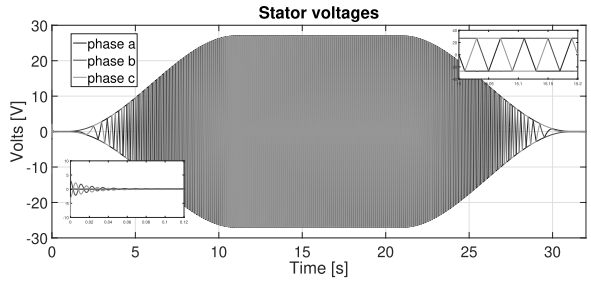

Fig. 9. Stator voltages without a load torque.

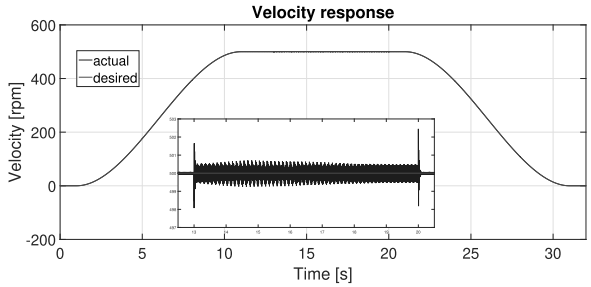

Fig. 10. Velocity response with a load torque.

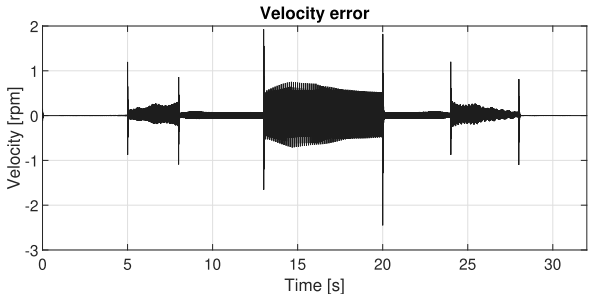

Fig. 11. Velocity error response with a load torque.

of the Fig. 7 that, at the beginning of the simulation, the current amplitudes of the two phases are required to be almost 0.88 A; these decrease in an oscillatory manner around 0 A, until reaching an amplitude of 0.1 A around 0.1 s. Therefore, the required current is well below the nominal values of the machine.

The current errors are mainly present in two phases of the stator windings, around 0.1 A at the beginning of the simulation, due to the initial condition that has been assumed; after (close 0.1 ms) the error is almost zero for the three currents as seen in the zoom box at the bottom left of Fig. 8. When the velocity of the BLDC motor reaches the desired angular velocity, the stator current errors reach values around 1.5 mA; if the desired velocity is equal to zero, such current errors reach values around 0.05 mA.

The control voltages applied to the BLDC motor are quasi-trapezoidal and, as the velocity reference increases, their frequency. This can be observed in the graphs shown in Fig. 9. The quasi-trapezoidal shape can be appreciated in the zoom box present in the figure. On the interval between 15 s and 15.2 s, the voltages reach an amplitude of 27 V at the maximum velocity reference. As can be seen, the voltages required by the motor are below the motor's nominal values. Also, in the zoom box at the bottom left of Fig. 9, it can be seen that two phases have an amplitude of approximately 10 V at the beginning of the simulation.

5.2. With a load torque. Although in the assumption S.5 the load torque is presumed to be a differentiable function of time, a second simulation is constructed using a non-differentiable step type function to emulate the rapid load changes that are sometimes experienced in practice. The experiment starts with a load torque of 0.1 Nm and changes in different moments to simulate that the shaft of the motor is coupled and uncoupled to an extra load using a clutch. Therefore, the load torque is given by

$$\tau_L = \begin{cases} 0.1, & 0 < t < 5, \\ 1, & 5 \leq t < 8, \\ 0.1, & 8 \leq t < 13, \\ 1.5, & 13 \leq t < 20, \\ 0.1, & 20 \leq t < 24, \\ 1, & 24 \leq t < 28, \\ 0.1, & 28 \leq t. \end{cases} \tag{66}$$

Also, for this simulation, the same desired velocity (64) and controller gains were used.

The velocity response, in this second experiment, at times when the motor does not have a load torque is the same as the previous one, as can be seen in Fig. 10. When the load torque is switched according to (66), the angular velocity response is oscillatory and presents peaks when the load engages and disengages. In the zoom box in Fig. 10 such peaks can be seen when the load torque of 1.5 Nm is applied in the time interval of 13 s to 20 s.

The velocity error is presented in Fig. 11, where it can be observed that the velocity error is around 0.3 rpm when the desired velocity changes and the load torque is engaged. When the maximum velocity is presented, the velocity error is approximately equal to 0.8 rpm. Two peaks of 1.93 rpm and -2.5 rpm appear when the load torque is engaged and disengaged, respectively. As can be seen, despite the fact that the controller is designed under the assumption S.5, the desired velocity is tracked with small oscillations due to the use of quasi-trapezoidal functions as in the first simulation.

The actual stator currents are the same as in the first simulation when no load torque is applied. In the intervals where the load torque is switched to be coupled with the shaft, the amplitude of the currents increases, as can be

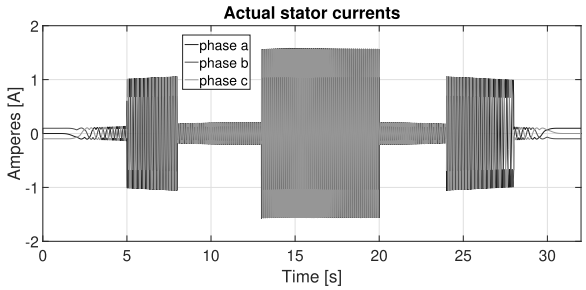

Fig. 12. Stator currents with a load torque.

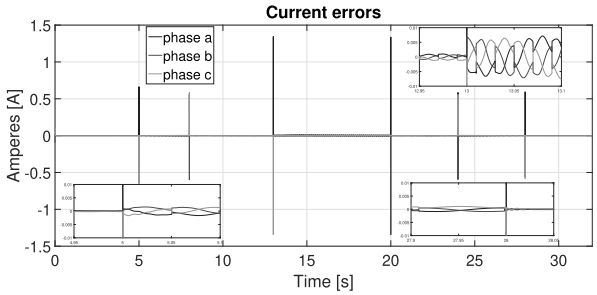

Fig. 13. Stator currents error with a load torque.

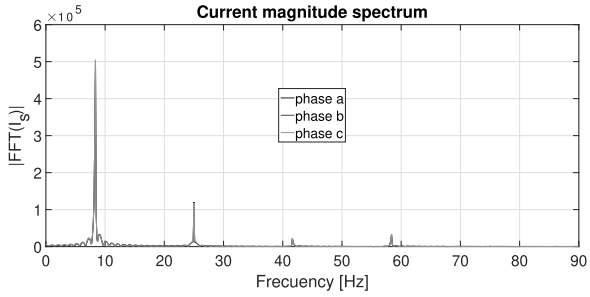

Fig. 14. Stator currents signals: the magnitude spectrum.

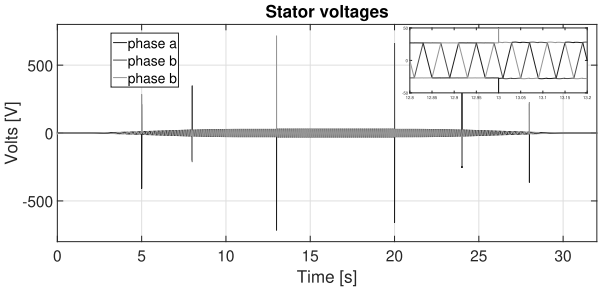

Fig. 15. Stator voltages with a load torque.

seen in Fig. 12. As expected, a larger load torque implies larger currents. When a 1 Nm load torque is applied, the stator currents reach 1 A, and obtain 1.5 A when a load torque of 1.5 Nm is applied.

The current errors are presented in Fig. 13. When the load torque is switched to coupled and uncoupled, a transient response is presented in the stator current errors, which is small when the time reaches 0.2 ms. When the load torque applied is 1 Nm and 1.5 Nm, the current errors reach 2 mA and 5 mA, respectively.

As can be seen in Fig. 12, when the velocity tracking is achieved, the currents have different amplitudes and frequencies, and quasi-trapezoidal signals with harmonic content are observed. Figure 14 presents a spectrum of the three current signals when they are in a steady state, from 12 to 20 seconds. It can be seen in this figure that, when the motor has a speed of 500 rpm, a frequency of around 8 Hz predominates.

Finally, after the load torque is switched, to coupled and uncoupled, the control voltages remain the same as when the load torque is constant after a brief transient. At the instants when the load torque is switched, there are voltage peaks of almost 300 V with a load torque of 1 Nm and 700 V with 1.5 Nm, but after 0.1 ms the voltages return to amplitude, equal to those presented in the simulation without a load torque, as can be observed in Fig. 15. The figure also presents a zoom box of the interval from 12.8 s to 13.2 s, which shows the quasi-trapezoidal shape of the voltages.

6. Conclusions

In this paper, an angular velocity control scheme for the BLDC motor was presented. The novel methodology takes advantage of the passivity properties of the mathematical model. In order to cope with the non-differentiability of EMF with a trapezoidal shape, a novel continuous and differentiable function was constructed to approximate EMF only using trigonometric functions. These quasi-trapezoidal functions were employed in the equations for the control voltages, the desired currents, as well as the derivatives of the latter. By using the angular position, the associated angular velocity was obtained through a linear second-order filter, which is employed in the whole of the proposed controller. A formal stability analysis of the complete closed-loop system was presented, which theoretically proves that the control objective is fulfilled and velocity is tracked without using velocity measurements.

It is worth noting that, from the results obtained from the second simulation, the controller may be able to handle discontinuous load torque functions. Therefore, future work will be centered on relaxing the assumption S.5 in the control scheme to formally include discontinuous functions in the design of the controller. Another topic of interest is the physical implementation of the proposal presented in this work.

Acknowledgment

The authors appreciate the support received from the TecNM projects and Universidad Autónoma de la Ciudad de México.

References

Carey, K.D., Zimmerman, N. and Ababei, C. (2019). Hybrid field oriented and direct torque control for sensorless BLDC motors used in aerial drones, *IET Power Electronics* **12**(3): 438–449.

Chiasson, J. (2005). *Modeling and High Performance Control of Electric Machines*, John Wiley & Sons, Hoboken.

de la Guerra, A., Alvarez-Icaza, L. and Torres, L. (2018). Brushless DC motor control with unknown and variable torque load, *IFAC-PapersOnLine* **51**(13): 644–649.

Gieras, J.F. (2009). *Permanent Magnet Motor Technology: Design and Applications*, CRC Press, Boca Raton.

Guerrero, C. and Santibañez, V. (2021). Simultaneous control of velocity and field flux of DC nonlinear motors, *IEEE Transactions on Industrial Electronics* **69**(3): 2322–2332.

Guerrero, C., Santibanez, V. and Ollervides, E.J. (2017). Control por retroalimentación de salida de un motor BLDC sin observador de estado de la velocidad angular, *Congreso Nacional de Control Automático, CNCA 2017, Monterrey, Mexico*, pp. 427–432.

Haddad, W.M. and Chellaboina, V. (2008). *Nonlinear Dynamical Systems and Control: A Lyapunov-based Approach*, Princeton University Press, Princeton.

Hajiaghasi, S., Salemnia, A. and Motabarian, F. (2017). Four switches direct power control of BLDC motor with trapezoidal back-EMF, *2017 8th Power Electronics, Drive Systems & Technologies Conference (PEDSTC), Mashhad, Iran*, pp. 513–518.

Hanselman, D.C. (2006). *Brushless Permanent Magnet Motor Design*, 2nd Edn, The Writers' Collective, Cranston.

Hernández-Guzmán, V.M. and Orrante-Sakanassi, J. (2021). PID control of robot manipulators actuated by BLDC motors, *International Journal of Control* **94**(2): 267–276.

Ioannou, P.A. and Sun, J. (1996). *Robust Adaptive Control*, Vol. 1, PTR Prentice-Hall, Upper Saddle River.

Jigang, H., Hui, F. and Jie, W. (2019). A PI controller optimized with modified differential evolution algorithm for speed control of BLDC motor, *Automatika: časopis za automatiku, mjerenje, elektroniku, računarstvo i komunikacije* **60**(2): 135–148.

Khazaee, A., Zarchi, H.A., Markadeh, G.A. and Hesar, H.M. (2020). MTPA strategy for direct torque control of brushless DC motor drive, *IEEE Transactions on Industrial Electronics* **68**(8): 6692–6700.

Kim, S.-H. (2017). *Electric Motor Control: DC, AC, and BLDC Motors*, Elsevier, Amsterdam.

Kommula, B.N. and Kota, V.R. (2020). Direct instantaneous torque control of brushless DC motor using firefly algorithm based fractional order PID controller, *Journal of King Saud University: Engineering Sciences* **32**(2): 133–140.

Krishnan, R. (2001). *Electric motor Drives: Modeling, Analysis, and Control*, Pearson, Upper Saddle River.

Maharajan, M.P. and Xavier, S.A.E. (2018). Design of speed control and reduction of torque ripple factor in BLDC motor using spider based controller, *IEEE Transactions on Power Electronics* **34**(8): 7826–7837.

Nam, K.H. (2018). *AC Motor Control and Electrical Vehicle Applications*, CRC Press, Boca Raton.

Salehifar, M. and Moreno-Equilaz, M. (2016). Fault diagnosis and fault-tolerant finite control set-model predictive control of a multiphase voltage-source inverter supplying BLDC motor, *ISA Transactions* **60**: 143–155.

Sova, V., Chalupa, J. and Grepl, R. (2015). Fault tolerant BLDC motor control for Hall sensors failure, *2015 21st International Conference on Automation and Computing (ICAC)*, Glasgow, UK, pp. 1–6.

Vorotnikov, V.I. (1998). *Partial Stability and Control*, Springer, Boston.

Xia, C.-l. (2012). *Permanent Magnet Brushless DC Motor Drives and Controls*, John Wiley & Sons, Singapore.

Cuauhtémoc Guerrero is a professor in the College of Science and Technology of UACM. He received his BS degree from Instituto Tecnológico de Saltillo, Mexico, in 1993, and his MS and PhD degrees from Universidad Nacional Autónoma de México, Mexico, in 2000 and 2006, respectively, all in electrical engineering. His research interests include electrical machine control, nonlinear systems control, and passivity-based control.

Víctor Santibañez received his PhD degree from CICESE, Ensenada, Mexico, in 1997. He is currently a professor and researcher with Instituto Tecnologico de la Laguna, Torreón, Coahuila, Mexico. He is an author or a coauthor of peer-reviewed journal articles and international conference papers. His research interests include robot and electromechanical devices control, nonlinear systems and adaptive control.

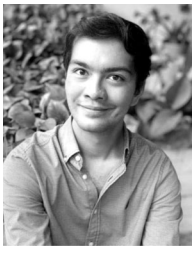

Jorge Villalobos-Chin holds a BE in mechatronics, and an MSc and PhD in electrical engineering from Instituto Tecnológico de la Laguna, Torreon, Coahuila, Mexico. His research interests include stability analysis, nonlinear control design and control of mechanical systems.

Jorge Orrante-Sakanassi received his BSc, MSc, and PhD degrees from Instituto Tecnologico de la Laguna, in 2006, 2008, and 2012, respectively. He was a postdoctoral fellow at Universidad Autónoma de Querétaro, from 2013 to 2015. Currently, he is a research professor with Tecnológico Nacional de Mexico/Instituto Tecnológico de La Laguna (since 2022), and has been a member of the Mexican Reserachers System (CONAHCYT SNII-Level 1) since 2018. His research interests are control of robot manipulators and electromechanical systems, modeling, nonlinear systems, and stability analysis. He has published a book, around 10 papers in international JCR indexed journals, and several papers in international and national conferences.

Javier Ollervides graduated in engineering electronics the TecNM/ITLaLaguna in 1996. Subsequently, he completed an MSc in electronics and telecommunications at the CICESE Research Center in Ensenada, Baja California, Mexico, in 2001. More recently, he obtained a doctorate in aeronautical engineering sciences from the CIIIA-FIME-UANL Research Center in San Nicolas de los Garza, Nuevo Leon, in 2021.

Received: 30 March 2025
Revised: 30 September 2025
Accepted: 4 November 2025